Title

Interfacial Jetting Phenomena Induced by Focused Surface Vibrations

Journal

Physical Review Letters, 103(2)

ISSN

0031-9007

Authors

Tan, Ming K

Friend, James R

Yeo, Leslie Y

Publication Date

2009-07-10

DOI

10.1103/physrevlett.103.024501

Peer reviewed

Interfacial Jetting Phenomena Induced by Focused Surface Vibrations

Ming K. Tan, James R. Friend, and Leslie Y. Yeo

Micro/Nanophysics Research Laboratory, Department of Mechanical Engineering, Monash University, Clayton, VIC 3800, Australia

(Received 29 September 2008; published 7 July 2009)

We exploit large accelerations associated with surface acoustic waves to drive an extraordinary fluid jetting phenomena. Laterally focusing the acoustic energy to a small region beneath a drop placed on the surface causes rapid interfacial destabilization. Above a critical Weber number We, an elongated jet forms for drops with dimensions greater than the fluid sound wavelength. Further increases in We lead to single droplet pinch-off and subsequent axisymmetric breakup to form multiple droplets. A simple equation based on a momentum balance is derived to predict the jet velocity.

DOI: 10.1103/PhysRevLett.103.024501 PACS numbers: 47.61.−k, 47.15.Uv, 47.55.N−, 68.35.Iv

Elongated liquid jets form beyond a critical Weber number when sufficient inertia exists to overcome the restoring capillary stresses acting on the interface of a liquid drop or meniscus [1]. Consequently, fluid confinement mechanisms such as nozzles or orifices are often necessary to accelerate the fluid to produce these jets. We demonstrate the unique generation of a liquid jet ejecting up to 1–2 cm from the free surface of a sessile drop without requiring such confinement. The key to the generation of such jetting phenomena is the concentration of mechanical energy into the drop made possible by surface acoustic waves.

We employ Rayleigh waves, 1–10 nm amplitude electroelastic surface acoustic waves (SAWs), that propagate along the substrate surface. SAWs and their energy are essentially confined to a depth of 3–4 wavelengths into the substrate, and the energy associated with these waves may be further concentrated to a spot with a size equivalent to the wavelength of the radiation using focusing transducers [2,3]. In doing so, large surface accelerations are formed—beyond 10^7 m/s^2—serving to destabilize the air-fluid interface of a drop set atop this surface and hence produce a single elongated column of liquid. This is in distinct contrast to the behavior induced by long-wavelength, in-phase piston vibration of a drop which can only atomize the drop via the formation and bursting of large numbers of short liquid spikes on the drop's surface [4]. A similar focusing concept but significantly different mechanism using a relatively large spherically converging acoustic beam has been employed to eliminate the use of nozzles [5]; the short focal depths in Ref. [5] result in short (<1 mm) jets which quickly pinch off to form an ejected droplet. Here, however, the acoustic radiation travels over a longer length scale in the fluid due to the SAW. Some cursory mention has been made of SAW-driven jets in the past [6], but little of the associated physics has been explored.

Figure 1 delineates the different fluid behavior observed when either a standing-wave or propagating SAW interacts with a liquid drop. The SAW is generated by applying a sinusoidal electric voltage to an interdigital transducer (IDT) fabricated on a 0.5 mm thick 128° y-x lithium niobate (LN) single crystal piezoelectric substrate [Fig. 1(a)]. The form of wave propagation is controlled through the boundary conditions along the wave propagation path; standing waves are obtained by allowing the wave to reflect off the free edges at either end of the substrate, while traveling waves are obtained by absorbing the acoustic energy with gel (polydimethylsiloxane or α-gel, GelTec Ltd., Japan). Details on the fabrication of the IDT are documented elsewhere [7,8]; the SAW wavelength $\lambda_{\mathrm{SAW}} \approx 200$ μm and frequency $f \approx 20$ MHz are set by the width and spacing between the IDT fingers since $c_s \approx 3990$ or 3974 m/s is the sound velocity in the substrate in the absence and presence of water loading, respectively. Regardless, the sound velocity in water is much less, $c_l \approx 1495$ m/s, causing a portion of the SAW—about 33% based on acoustic impedances—to refract into the liquid drop at an angle known as the Rayleigh angle $\theta_{\mathrm{SAW}} = \sin^{-1} c_l/c_s \approx 23°$. At sufficient intensities, the so-called leaky SAW in the liquid, in turn, generates acoustic streaming and bulk flow within the drop [3,9], with the air-water interface representing a reflective boundary for the acoustic radiation due to the large acoustic impedance difference across it.

At relatively low applied powers and hence low surface acceleration $|\ddot{\xi}_{x_3}|$, where $\ddot{\xi}$ represents the second-order time derivative of the substrate's surface displacement ξ and x_3 the direction perpendicular to the substrate, weak acoustic streaming will occur in drops with sizes much greater than the acoustic wavelength in the fluid, i.e., $R_d \gg \lambda_f \sim 73$ μm for $f \approx 20$ MHz. However, as the drop sizes shrink, capillary stresses begin to dominate, and capillary waves begin to appear on the drop interface. As the drop becomes progressively smaller, the intensity of these vibrations grows (provided $R_d \gg \lambda_c \sim 1$ μm, which is the capillary wavelength), while the streaming weakens as a result of the increasing surface-to-volume ratio as R_d decreases; the capillary waves depend upon the surface area, while the acoustic streaming depends upon the volume. When $R_d \approx \lambda_f$, the streaming within the drop ceases. A qualitative summary of the different fluid responses

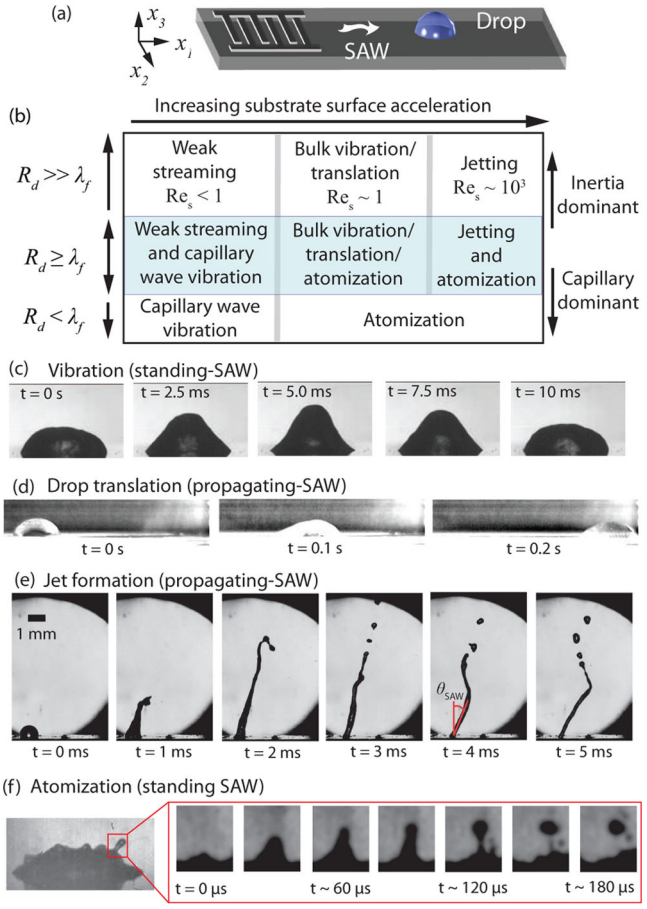

FIG. 1 (color online). (a) Illustration of the SAW device on which a 3 μl deionized water drop is placed in the propagation pathway of the SAW. A standing SAW naturally arises due to reflection off the edges of the substrate. If a propagating SAW is desired, α-gel is placed along the edges to absorb the radiation, preventing reflection. (b) Summary of the different drop behaviors observed as a function of the surface acceleration magnitude and the drop size: (c) drop vibration due to standing SAW, (d) drop translation due to propagating SAW, (e) jetting at the Rayleigh angle θ_{SAW} as a consequence of propagating SAW irradiation, and (f) drop atomization due to a standing SAW.

based on the acceleration magnitude and drop size is provided in Fig. 1(b).

With increasing power, the increasing surface acceleration magnitude on the substrate $|\ddot{\xi}_{x_3}|$ leads to stronger fluid streaming, as characterized by the streaming Reynolds number $\mathrm{Re}_s \equiv \rho U_s R_d/\mu$, where ρ and μ are the liquid density and viscosity, respectively, and U_s is the characteristic streaming velocity. For $\mathrm{Re}_s \sim 1$, $U_s \sim 10^{-3}$ m/s. Bulk vibration of the drop is also observed [Fig. 1(c)] when a standing SAW is employed. At these powers, the acoustic streaming in the drop generates sufficient body force to overcome contact line pinning, and the drop begins to translate if the SAW is propagating [Fig. 1(d)] [7]. With further increases in $|\ddot{\xi}_{x_3}|$, the inertial streaming ($\mathrm{Re}_s \sim 10^3$) can no longer be dissipated by viscous or capillary means, and the drop either deforms into an elongated liquid jet [Fig. 1(e)] or atomizes [Fig. 1(f)] [8]; note the asymmetric deformation of the drop and the formation of the jet at the Rayleigh angle in Fig. 1(e). At a given value of $|\ddot{\xi}_{x_3}|$, we observe jets forming in the inertia dominant regime when $R_d \gg \lambda_f$, while atomization is particularly prominent in the capillary force dominant regime when $R_d < \lambda_f$, as summarized in Fig. 1.

Given that the drop vibration, translation, streaming, and atomization phenomena have been studied separately, we will restrict our emphasis in the rest of this Letter to the peculiar jetting phenomenon. To confine the radiation intensity to a point on the substrate, we employ a pair of elliptical focusing transducers as shown in Fig. 2(a), specifically known as electrode-width-controlled, single-phase unidirectional transducers (EWC-SPUDTs, hereafter referred to as electrodes).

The 30 MHz electrodes, consisting of an array of curved narrow strips of metal, are fabricated on LN substrates using UV photolithography [3]. Internally tuned reflectors within the electrodes enable unidirectional SAW propaga-

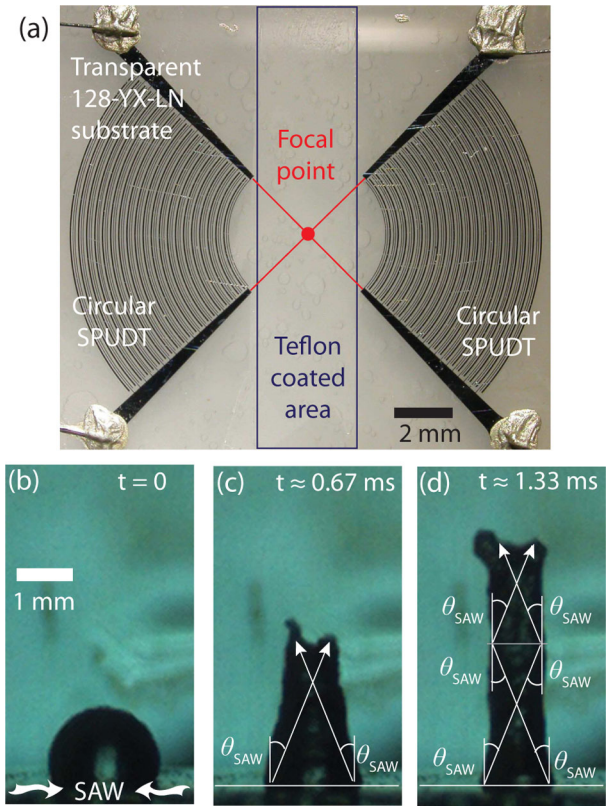

FIG. 2 (color online). Image (a) shows two circular focusing electrode-width-controlled SPUDTs fabricated at the ends of a LN substrate to provide the focused SAWs whose radiation into the drop placed on the substrate causes it to deform into a coherent elongated jet as shown in images (b)–(d). The water-air interface reflects the acoustic radiation up the fluid column as it extends, as depicted in image (d). The drop is placed at the focal point between the two EWC-SPUDTs within an area coated with a thin (<1 μm) layer of Teflon to render the hydrophilic LN substrate hydrophobic.

tion toward the focal point shown in Fig. 2(a), and a strong standing-wave SAW is generated through the superposition of focused SAWs that propagate along the x axis from the aligned electrodes at both ends of the substrate. To increase the static contact angle between the deionized water drop (here 1, 3, and 5 μl drop volumes V_d are employed) and the substrate surface, we coat an area on the substrate in between the electrodes, as shown in Fig. 2(a), with a 100 nm thick layer of Teflon (Teflon AF, DuPont Corp., USA). The jetting dynamics were captured at 500–2000 fps using a high speed video camera (iSpeed, Olympus, Japan) mounted onto a long-distance microscope (K2, InfiniVar, USA). Measurements of the surface acceleration $\ddot{\xi}_{x_3}$ were obtained through scanning laser Doppler vibrometry (MSA-400, Polytec PI, Germany) focused directly on the substrate. A movie showing a typical jetting event is given in the supplementary information [10].

Figure 3(a) shows the jet length prior to its breakup as a function of the driving force $F = \rho V_d \ddot{\xi}_{x_3}$. We note the large magnitudes due to the high surface accelerations afforded by the SAW, which facilitates the transmission of the acoustic energy into the drop as discussed above. At the input powers employed, the surface displacement velocity $\dot{\xi}_{x_3}$ is around 1 m/s irrespective of the SAW excitation frequency. So while the surface displacement ξ_{x_3} and hence the SAW amplitude are only around 10 nm at these 10 MHz order frequencies, the surface acceleration is on the order 10^8 m/s^2 [8]. It is these extremely large accelerations which are transmitted into the drop through an area on the order of λ_{SAW} in size via radiation focusing that give rise to the jetting phenomena. There exists a threshold value for the force that, once exceeded, causes jetting; the larger the parent drop, the larger the threshold value. Below the threshold, the drop merely vibrates with an amplitude proportional to the force, as depicted in Fig. 1(c), since there is insufficient inertial stress to overcome the surface tension of the drop. In fact, the threshold value for the force at the onset of jetting actually sets the jet length. At the onset of jetting, a balance between the surface energies of the parent drop, assumed hemispherical due to the hydrophobic substrate, and the jet, assumed to resemble a cylindrical column, then sets the length of the jet when it first appears from the conical apex of the vibrating drop after

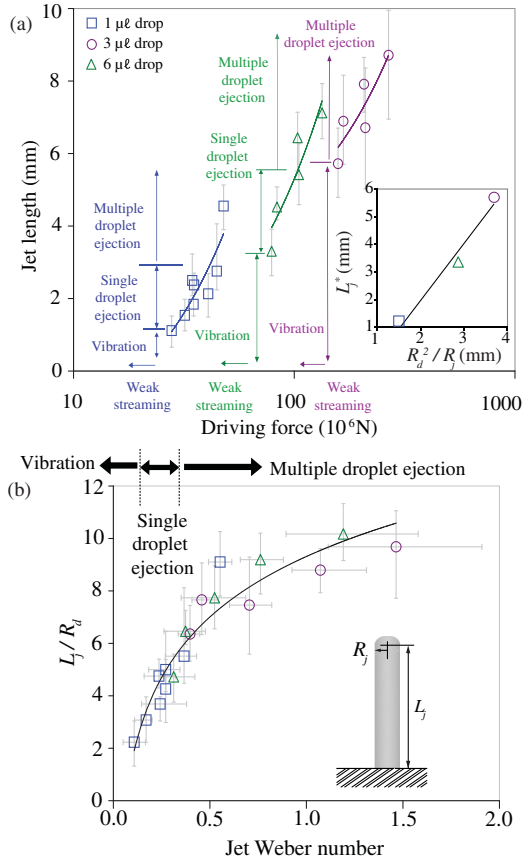

FIG. 3 (color online). (a) Jet length as a function of the driving force. The inset shows the jet length at the onset of the phenomena at the instant when the threshold force exceeds L_j^* (the jet length at the smallest value of the driving force when jetting is first observed) and its relationship to the parent drop size. (b) Dimensionless jet length as a function of the jet Weber number. We note the transitions for both the onset of jetting from drop vibration and between single and multiple droplet ejections occur at Weber numbers of 0.1 and 0.4, respectively.

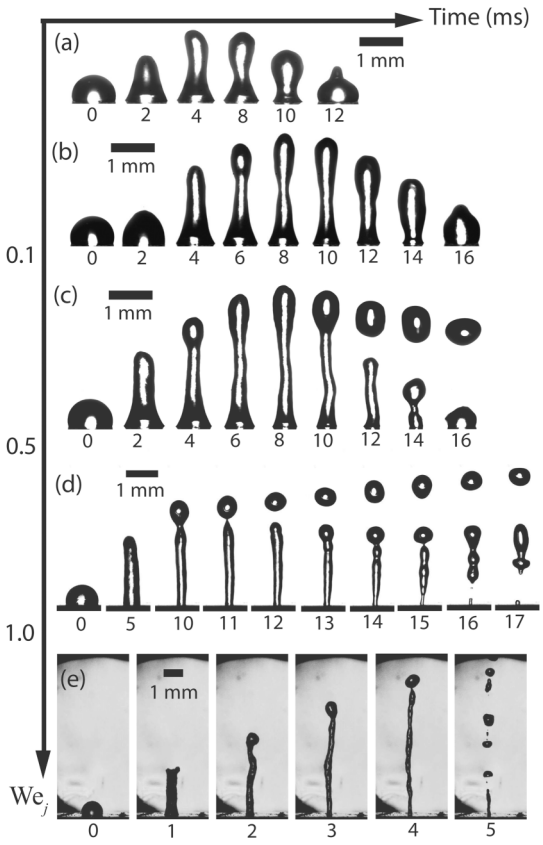

FIG. 4. Experimental images showing the transition from (a) drop vibration to (b) jetting, (c) pinch-off of a single droplet, and (d),(e) jet breakup to form multiple droplets by increasing the jet Weber number We_j.

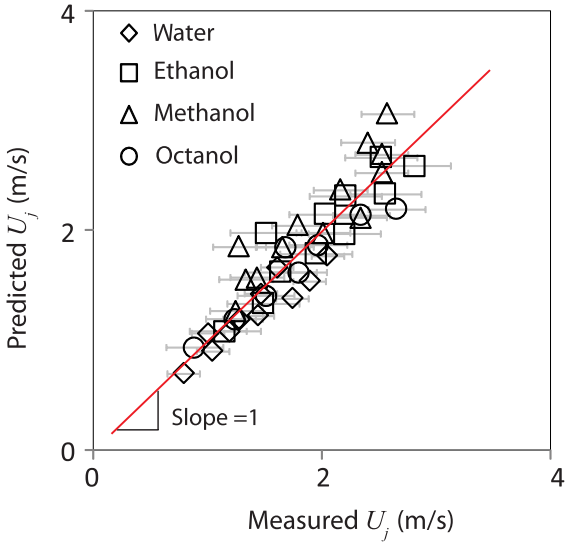

FIG. 5 (color online). Comparison between the experimentally measured jet velocity with the prediction given by Eq. (1).

the threshold force is exceeded: $L_j^* \sim R_d^2/R_j$, in which R_j is the jet radius, consistent with that observed in the inset in Fig. 3(a).

Figure 3(a) also documents evidence that, at larger driving forces, the jet no longer pinches off at its leading edge to eject a single droplet. Instead, we see evidence of the classical Rayleigh-Plateau instability through which the cylindrical liquid column becomes unstable to axisymmetric perturbations with wavelengths several times larger than the R_j [11], consequently breaking up to form multiple droplets. The transitions from the onset of jetting to the pinch-off of a single droplet and the breakup of the jet to form multiple droplets are more clearly observed by recasting the experimental data in terms of a jet Weber number $\mathrm{We}_j \equiv \rho U_j^2 R_j/\gamma$, where U_j is the velocity of the jet, as shown in Fig. 3(b). We observe the onset of jetting and the transition from single droplet pinch-off to multiple droplet formation as a consequence of the axisymmetric breakup of the jet to universally occur at Weber numbers of 0.1 and 0.4, respectively. Typical dynamics of the jet formation and the droplet ejection at different Weber numbers captured through high speed flow visualization are shown in Fig. 4.

By introducing an acoustic forcing term to the leading order axisymmetric jet momentum balance derived by Eggers [1], we arrive at the following relationship that permits the prediction of the axial jet velocity:

$$U_j \cong [2L_j(F_s^y - g)]^{1/2}, \qquad (1)$$

where $F_s^y \approx \alpha_0 \beta \dot{\xi}_{x3}^2 \mathrm{Re}_A$ is the force associated with the acoustic streaming in the jet and g is the gravitational acceleration. $\mathrm{Re}_A = \rho \dot{\xi}_{x_3} \lambda_f/(2\pi b)$ is the acoustic Reynolds number [12] in which $b = 4\mu/3 + \mu_B$, μ_B being the bulk viscosity of the fluid. $\alpha_0 = \pi b f/(\rho c_l^3)$ is the acoustic attenuation coefficient, and $\beta = 1 + B/2A$ is the coefficient of nonlinearity; experimental values of B/A for various liquids are given in Ref. [13]. The full derivation of Eq. (1) can be found in Ref. [14]; we note that by assuming the radius and radial velocity of the jet to be constant along its elongation axis, which is reasonable given the observations in Figs. 2 and 4, the jetting dynamics has been rendered independent of the surface tension, whereas the viscosity appears only through the acoustic forcing as a dissipative sink. Figure 5 shows the good agreement obtained between the prediction afforded by Eq. (1) and the experimental data for various fluids.

We are grateful to an anonymous referee for extremely helpful suggestions with regards to the jet theory.

[1] J. Eggers, Rev. Mod. Phys. **69**, 865 (1997).
[2] M. K. Tan, J. R. Friend, and L. Y. Yeo, Appl. Phys. Lett. **91**, 224101 (2007); V. Laude, D. Gérard, N. Khelfaoui, C. F. Jerez-Hanckes, S. Benchabane, and A. Khelif, Appl. Phys. Lett. **92**, 094104 (2008).
[3] R. Shilton, M. K. Tan, J. R. Friend, and L. Y. Yeo, J. Appl. Phys. **104**, 014910 (2008).
[4] A. J. James, B. Vukasinovic, M. K. Smith, and A. Glezer, J. Fluid Mech. **476**, 1 (2003).
[5] S. Elrod, B. Hadimioglu, B. Khuri-Yakub, E. Rawson, E. Richley, C. Quate, N. Mansour, and T. Lundgren, J. Appl. Phys. **65**, 3441 (1989).
[6] K. Chono, N. Shimizu, Y. Matsui, J. Kondoh, and S. Shiokawa, Jpn. J. Appl. Phys. **43**, 2987 (2004); A. Renaudin, P. Tabourier, V. Zhang, J. C. Camart, and C. Druon, Sens. Actuators B Chem. **113**, 389 (2006).
[7] M. K. Tan, J. R. Friend, and L. Y. Yeo, Lab Chip **7**, 618 (2007).
[8] A. Qi, L. Y. Yeo, and J. R. Friend, Phys. Fluids **20**, 074103 (2008).
[9] T. Frommelt, M. Kostur, M. Wenzel-Schäfer, P. Talkner, P. Hänggi, and A. Wixforth, Phys. Rev. Lett. **100**, 034502 (2008); H. Li, J. R. Friend, and L. Y. Yeo, Phys. Rev. Lett. **101**, 084502 (2008).
[10] See EPAPS Document No. E-PRLTAO-103-019930 for a movie of a typical jetting event. For more information on EPAPS, see http://www.aip.org/pubservs/epaps.html.
[11] J. Plateau, Acad. Sci. Bruxelles Mém. **23**, 5 (1849); Lord Rayleigh, Proc. R. Soc. London **29**, 71 (1879).
[12] L. D. Rozenberg, *High-Intensity Ultrasonic Fields* (Plenum, New York, 1971).
[13] R. T. Beyer, in *Nonlinear Acoustics*, edited by M. F. Hamilton and D. T. Blackstock (Academic, New York, 1998).
[14] See EPAPS Document No. E-PRLTAO-103-019930 for the full derivation. For more information on EPAPS, see http://www.aip.org/pubservs/epaps.html.